DOI: 10.17344/acsi.2020.6183 *Acta Chim. Slov.* **2021,** *68,* 88–101

Scientific paper

Synthesis, Crystallographic Structure, Hirshfeld Surface Analysis, Drug-likeness Properties and Molecular Docking Studies of New Oxime-pyridine Compounds

Tufan Topal*

Department of Chemistry, Pamukkale University, 20020, Denizli, Turkey,

** Corresponding author: E-mail: tufantopal@hotmail.com*
Phone: +90 258 2963457, fax: +90 258 2963535

Received: 06-11-2020

Abstract

A detailed description of the two new pyridine ligands, (2E,3Z)-3-[2-(3-chloropyridin-2-yl)hydrazinylidene]-N-hydroxybutan-2-imine and 3-chloro-2-{(2Z)-2-[1-(4 nitrophenyl)ethylidene]hydrazinyl}, is reported. The synthesized compounds were characterized by spectroscopic studies, spectral features were performed by TD-DFT calculations. New-generation pyridine ligand of HL_2 was also determinate by single-crystal X-ray diffraction and Hirshfeld surface analysis with two-dimensional fingerprint plots was used to analyze intermolecular interactions in crystals. Molecular-docking was performed to investigate the binding areas of chemical compounds, and the results showed the inhibitory activity of the studied HL_1 and HL_2 against *E. coli***.** The results of the current study revealed the drug-likeness and bioactive properties of the ligands.

Keywords: Pyridine-oxime; molecular electrostatic potential (MEP); Drug-likeness; E. Coli; Hirshfeld surface analysis; X-ray diffraction

1. Introduction

For biological activities, pyridine compounds are widely used as antibacterial, antifungal, and anticancer agents.[1–3] Several studies have been conducted on biological compounds in health-related journals and books. Accordingly, pyridine derivatives cause interactions with high binding capacity by targeting enzymes, proteins, and deoxyribonucleic acid (DNA) that create biological problems.[4] With the discovery of new compounds, several studies were performed in the last decade to inhibit antibacterial drug resistance and reduce associated adverse effects on human health.[5] It is clear that new types of viruses and bacteria affect the lives of humans worldwide in a variety of ways. Accordingly, this places immense responsibility on researchers and chemists who work to develop new materials to decrease the effects of viruses and bacteria as well as biologists and physicians who test the new compounds on animals and humans. Requiring extensive research, conducting in vitro studies is costly and time-consuming; accordingly, one of the most important advantages of the current study was the contribution to perform *in silico* studies inactivating viruses, bacteria, and cancer cells by the production of ligands with medicinal potential. Pyridine and oxime compounds have a high interference of hydrogen bond in electrostatic potential capacity. Intramolecular and intermolecular hydrogen bonds play a major role in the interacting and binding of biological molecules. In addition, pyridine and oxime compounds have been selected particularly for their ability to easily transfer the electrons of nitrogen atoms participating in the aromatic ring and C=N groups into the donor–acceptor system.[6–11] Due to their high levels of antibacterial properties and bioactive multizones, nitrogenous organic or inorganic compounds are reported to have positive effects on *Escherichia coli.*[12] The reason for the investigation of *E. coli* pathogens in molecular-docking studies is this bacterium's resistance against some medications and its high binding capacity.[5] Furthermore, *E. coli,* also known as the most-common human pathogen, causes different types of infections, such as kidney, gallbladder, skin, and respiratory infections in addition to meningitis in neonates.[13,14] The physicochemical properties of compounds affect bioavailability, including electrostatic potential, molar absorptivity, stability, solubility, structure, intracellular absorption, hydrogen bonds, and bonding energy.[15,16] The theoretical method such as Density Functional Theory (DFT) in the computational chemistry is

important tool to predict the assignment of specific electronic transitions in the UV-Vis spectra. In the present study, oxime and pyridine derivative compounds were synthesized and characterized by X-ray and spectroscopic methods. In addition, the surface analysis was performed to analyze their chemical properties, and molecular electrostatic potential was calculated to determine the nucleophilic and electrophilic zones. Molecular-docking was conducted to investigate the hydrogen-binding interactions of *E. coli* DNA gyrase subunit B (GyrB) and *E. coli* beta-ketoacyl-acyl carrier protein synthase III (FabH) and determined pharmacokinetic and pharmacological properties.

2. Materials and Methods

2. 1. Materials and Physical Measurements

The chemicals and solvents: methanol, acetonitrile, 3-chloro-2-hydrazinopyridine, 2,3 butanedione monoxime, 4′-nitroacetophenone were obtained from Sigma–Aldrich. BRUKER BIOSPIN NMR AVANCE Spectrometer III 400MHz model spectrometer was used for ^{1}H-NMR and ^{13}C-NMR analysis. Elemental analysis were determined using a Costech Elemental analysis device ECS 4010 Model analyzer. IR spectrums were recorded in the 400–4000 cm^{-1} on Perkin Elmer FTIR-Spectrometer Spectrum Two Model and Mass Spectra (ESI) on TSQ Fortis™ Triple Quadrupole Mass Spectrometer. Melting points of ligands were determined by Stuart SMP10. The mains water was passed through the Thermo Scientific Smart2pure device to make it pure water. Absorption spectra was carried out using Shimadzu UV-1800 UV-VIS spectrophotometer. Single-crystal X-ray structure was determined using an Agilent SuperNova Dual CCD detector diffractometer eguipped with graphite-monochromated MoKα radiation (λ = 0.71073 °A) at room temperature.

2. 2. Synthesis of Ligands HL_1, HL_2

Chemical preparation of (2*E*,3*Z*)-3-[2-(3-chloropyridin-2-yl)hydrazinylidene]-*N*-hydroxybutan-2-imine HL_1 and 3-chloro-2-{(2*Z*)-2-[1-(4-nitrophenyl)ethylidene]hydrazinyl}pyridine HL_2.

3-chloro-2-hydrazinopyridine (1 mmol, 0.1435 g) in acetonitrile solution (10 ml) was added 2,3 butanedione monoxime (1 mmol, 0.1011 g) HL_1 and 4′-Nitroacetophenone (1 mmol, 0.1651 g) HL_2 in 10 ml of acetonitrile respectively (Fig.1). The both solution stirred for 24 h at room temperature and were kept aside for slow evaporation of solvent for about 5 days. The HL_2 crystal was obtained from slow evaporation technique by dissolving the product in acetonitrile.

$C_9H_{11}ClN_4O$ (HL_1), Crem; Yield 87%. m.p.:194 °C. ^{1}H-NMR (400 MHz, Chloroform-d_6, ppm): δ 9.83 (s, 1H, O-H), δ 8.45 (s, 1H, -NH), δ 8.37 (d, 1H, Ar-H), δ 7.62 (d, 1H, Ar-H), δ 6.84 (t, 1H, Ar-H), δ 2.34 (s, 3H, -CH_3), δ 2.23 (s, 3H, -CH_3). ^{13}C-NMR (100 MHz, Chloroform-d_6, ppm): δ 157.39 (-C=N-OH), δ 157.32 (-C=N-), δ 150.00, 147.12, 137.32, 116.50, 115.35 (C-$Ar_{pyridine}$), δ 10.03 (-CH_3), δ 9.53 (-CH_3).[17] LC/MS-MS, (ESI) m/z= 226.66284 $[M+1]^+$ (100%). Calcd. for $C_9H_{11}ClN_4O$: C, 47.69; H, 4.89; N, 24.72%; found: C, 47.71; H, 4.86; N, 24.69%. IR (KBr) cm^{-1}: 3357 (N-H), 3112 (O-H), 2981 (C-H_{Ar}), 1596 (C=N)$_{pyridine}$, 1561 (C=N)$_{imine}$, 1516 (C=N)$_{oxime}$, 935 (N-O).

$C_{13}H_{11}ClN_4O_2$ (HL_2), Orange; Yield 86%. m.p.:169 °C. ^{1}H-NMR (400 MHz, Chloroform-d_6, ppm): δ 8.48 (s, 1H, -NH), δ 8.30 (d, 1H, Ar-H), δ 8.20 (d, 2H, Ar-H), δ 8.01 (d, 2H, Ar-H), δ 7.61 (d, 1H, Ar-H), 6.84 (t, 1H, Ar-H), δ 2.38 (s, 3H, -CH_3), ^{13}C-NMR (100 MHz, Chloroform-d_6, ppm): δ 149.92, δ 147.61 (C-$Ar_{pyridine}$), δ 147.17 (-C=N-), δ 144.49, 144.42 (C-Ar), δ 137.33 (C-$Ar_{pyridine}$), δ 126.89, 126.89, 123.64, 123.64 (C-Ar), δ 116.97, 115.49 (C-$Ar_{pyridine}$), δ 12.53 (-CH_3). LC/MS-MS, (ESI) m/z= 290.70558

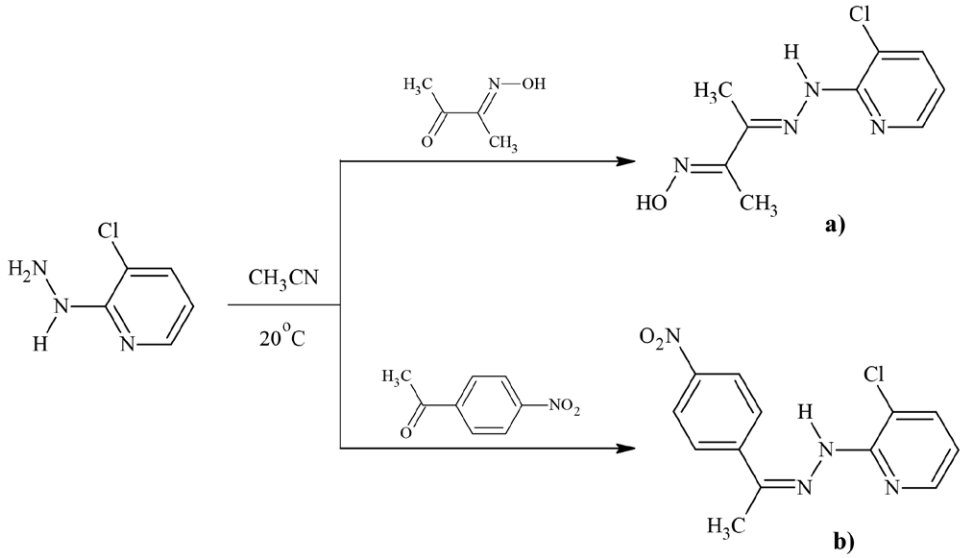

Fig. 1. Structure of compounds a) HL_1 and b) HL_2

$[M+1]^+$ (100%). Calcd. for $C_{13}H_{11}ClN_4O_2$: C, 53.71; H, 3.81; N, 19.27%; found: C, 53.73; H, 3.79; N, 19.22%. IR (KBr) cm^{-1}: 3378 (N-H), 2922 (C-H_{Ar}), 1585 (C=N) $_{pyridine}$, 1557 $(C=N)_{imine}$, 1392 (NO_2).[18]1H NMR and UV-Vis spectra. Reaction of 1:1 stoichiometric proportion of HL with Na2[PdCl4] in methanol affords a mononuclear palladium(II

2. 3. X-ray Crystallography Analysis

Orange crystal of the $C_{13}H_{11}ClN_4O_2$ compound was obtained in acetonitrile solution through slow evaporation for 5 days at room temperature. The data set of reflections were collected using an Agilent SuperNova X-Ray diffractometer with MoKα (λ = 0.71073) at 293 K. The data reduction and data correction were performed by Olex2 software (version 1.3).[19,20] Refinements were obtained by the Full-Matrix method on F^2 using the Olex2 software, and crystal packing diagrams were created by Mercury 4.3.0 software. All the nonhydrogen atoms were anisotropically refined using the riding model approximation.[21] Tables 1 and 2, a summary of the experimental details of HL_2.[22–24] CCDC DOI: 10.5517/ccdc.csd.cc24rlzh and number 1988897 contains the supplementary rystallographic data for this work. This data can be obtained from The Cambridge Crystallographic Data Centre via www.ccdc.cam.ac.uk/data_ request/cif.

Table 1. Crystal data and structure refinement for HL_2.

CCDC number	1988897
Empirical formula	$C_{13}H_{11}ClN_4O_2$
Formula weight	290.71
Temperature/K	293(2)
Crystal system	monoclinic
Space group	$P2_1/c$
a/Å	11.7767(7)
b/Å	14.4529(7)
c/Å	7.9073(4)
α/°	90
β/°	91.381(5)
γ/°	90
Volume/$Å^3$	1345.49(12)
Z	4
$\rho_{calc}g/cm^3$	1.435
μ/mm^1	0.291
F(000)	600.0
Crystal size/mm^3	0.14 × 0.13 × 0.12
Radiation	Mo Kα (λ = 0.71073)
2Θ range for data collection/°	6.756 to 49.996
Index ranges	$-8 \le h \le 14$, $-16 \le k \le 16$, $-8 \le l \le 9$
Reflections collected	4286
Independent reflections	2343 [R_{int}=0.0161, R_{sigma} = 0.0302]
Data/restraints/parameters	2343/0/182
Goodness-of-fit on F^2	1.047
Final R indexes [I>=2σ (I)]	R_1 = 0.0548, wR_2 = 0.1338
Final R indexes [all data]	R_1 = 0.0790, wR_2 = 0.1491
Largest diff. peak/hole / e $Å^{-3}$	0.21/-0.41

3. Results and Discussion

3. 1. Description of the Crystal Structures and Hydrogen Bonding

Slow evaporation technique was used to make the sample suitable for X-ray structure analysis. The HL_2 crystallizes in the centrosymmetric space group $P2_1/c$ of monoclinic system with a unit cell volume of 1345.49(12) $Å^3$, the cell dimensions are: a = 11.7767(7) Å, b = 14.4529(7)

Table 2. Selected Bond Lengths/Å, Angles/° and Torsion/° for HL_2.

Atom	Atom	Length	Atom	Atom	Atom	Angle	Atom	Atom	Atom	Atom	Torsion
N7	N8	1.355(3)	C9	N8	N7	117.57(19)	N7	N8	C9	C10	–1.6(3)
N8	C9	1.287(3)	N8	N7	C2	121.4(2)	N8	N7	C2	N1	–1.4(4)
N1	C2	1.329(3)	C2	N1	C6	117.2(3)	C2	N1	C6	H6	–179.5(4)
N1	C6	1.333(4)	C13	C12	C9	120.2(2)	C13	C12	C9	N8	8.3(3)
C9	C12	1.474(3)	C17	C12	C9	122.1(2)	C9	N8	N7	H7	–4.3(4)
C12	C13	1.397(3)	C17	C12	C13	117.7(2)	C2	N7	N8	C9	175.7(2)
C12	C17	1.391(3)	N1	C2	C3	122.5(2)	C6	N1	C2	N7	–177.6(3)
C3	C2	1.394(4)	C4	C3	C2	118.7(3)	C6	N1	C2	C3	2.4(4)
C9	C10	1.505(3)	C12	C9	C10	120.8(2)	C10	C9	C12	C13	–170.9(2)
C14	C13	1.375(3)	N8	C9	C12	115.0(2)	N8	C9	C12	C17	–172.1(2)
C17	C16	1.369(4)	N8	C9	C10	124.2(2)	C10	C9	C12	C17	8.7(3)
C15	C14	1.379(4)	N7	C2	C3	118.7(2)	N8	C9	C10	10HA	–55.3
C4	C3	1.375(4)	C16	C17	C12	122.0(2)	N8	C9	C10	10HB	–175.3
C6	C5	1.368(5)	N1	C2	N7	118.9(2)	N8	C9	C10	10HC	64.7
C5	C4	1.371(5)	N1	C6	C5	124.2(3)	C12	C9	C10	10HA	123.9
N7	C2	1.371(3)	C14	C15	N18	119.1(3)	C12	C9	C10	10HB	3.9
C16	C15	1.361(4)	C14	C13	C12	120.6(2)	C12	C9	C10	10HC	–116.1

Å, c = 7.9073(4) Å, β = 91.381(5)° and Z = 4. The full data collection was done for indices h, k and l with ranges of -8 ≤ h ≤ 14, −16 ≤ k ≤ 16, −8 ≤ l ≤ 9 and R value of R_1 = 0.0548, wR_2 = 0.1338. Carbon and hydrogen atoms have been geometrically positioned.

The bond lengths between the atoms N8=C9 1.287(3) Å, N7-N8 1.355(3) Å, C9-C12 1.474(3) Å, C12-C13 1.397(3) Å and C12-C17 1.391(3) Å were found. In literature 1.28(14) Å, 1.35(3) Å, 1.49(14) Å, 1.39(15) Å and 1.38(16) Å are similar with our values of atomic lengths.[25–27] The N8=C9 bond was shorter than the N8-N7 bond and it confirms that N8=C9 shows a double bond character. In HL_2, pyridyl N1-C2 and N1-C6 bond distances were 1.329(3) and 1.333(4) Å, bond angle C2-N1-C6 117.2(3)° and torsion angle C2-N1-C6-H6 -179.5(4)° were found and this torsion value is competible with the expected 180°.[11,28] Torsion angles of atoms between pyridyl and benzene ring have been observed C13-C12-C9-N8 8.3(3)°, N8-N7-C2-N1 −1.4(4)° and N7-N8-C9-C10 −1.6(3)°. The ORTEP-3 drawn with 35% probability is given in Fig. 2.

Basically 3 pairs of hydrogen bond interactions are observed in the structure, these are C-H···O, C-H···N and C-H···Cl intramolecular and intermolecular hydrogen bonds.[29,30] Selected hydrogen bond distances and angles are listed in Table 3. In HL_2, carbon atom C10 acts as a donor to N1 atom at C(10)-H(10A)···N(1) (x,1.5-y,-1/2+z),

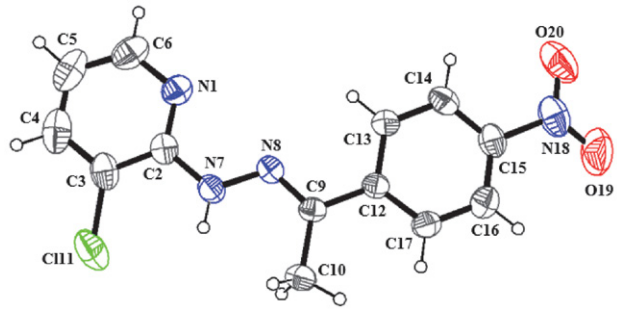

Fig. 2. Molecular structure of the HL_2. Thermal ellipsoids are shown at 35% probability level

developing the capped stick style and two-dimensional chain along the crystallographic axis as depicted in Fig. 3a.

As illustrated in Fig. 3b, in HL_2, C-H···O intermolecular hydrogen bonding interactions were used to generate a three-dimensional (3D) supramolecular network along the c axis. All the figures were drawn in Mercury software. Other hidrogen bonds were C(10)-H(10A)···Cl(11) (1-x,2-y,1-z), C(5)-H(5)···O(20) (1-x,1-y,1-z), C(10)-H(10B)···O(19) (2-x,-1/2 + y,1/2-z), C(17)-H(17) ···O(20) (2-x,-1/2 + y,1/2-z), C(5)-H(5)···O(19) (-1 + x,y,1 + z), C(10)-H(10B)···O(20) (2-x,-1/2 + y,1/2-z), C(13)- H(13)···Cl(11) (1-x,2-y,1-z).[31]

Table 3. Selected hydrogen bond distances (Å), symmetry and angles (°) for HL_2.

D-H···Å	d (D-H)	d (H···Å)	d(D-H···Å)	Symmetry codes	∠D–H···Å
C(10)-H(10A)···Cl(11)	0.960	3.174	3.882	1-x,2-y,1-z	131.90
C(10)-H(10A) ···N(1)	0.960	2.768	3.602	x,1.5-y, -1/2+z	145.68
C(5)-H(5)···O(20)	0.930	3.019	3.606	1-x,1-y,1-z	122.57
C(10)-H(10B)···O(19)	0.960	2.730	3.417	2-x, -1/2+y,1/2-z	129.08
C(17)-H(17)···O(20)	0.930	2.460	3.322	2-x, -1/2+y,1/2-z	154.19
C(13)-H(13) ···Cl(11)	0.930	2.941	3.764	1-x,-1/2+y,1.5-z	148.37
C(5)-H(5)···O(19)	0.930	2.909	3.747	-1+x,y,1+z	150.54
C(10)-H(10B)···O(20)	0.960	3.057	3.978	2-x, -1/2+y,1/2-z	161.22

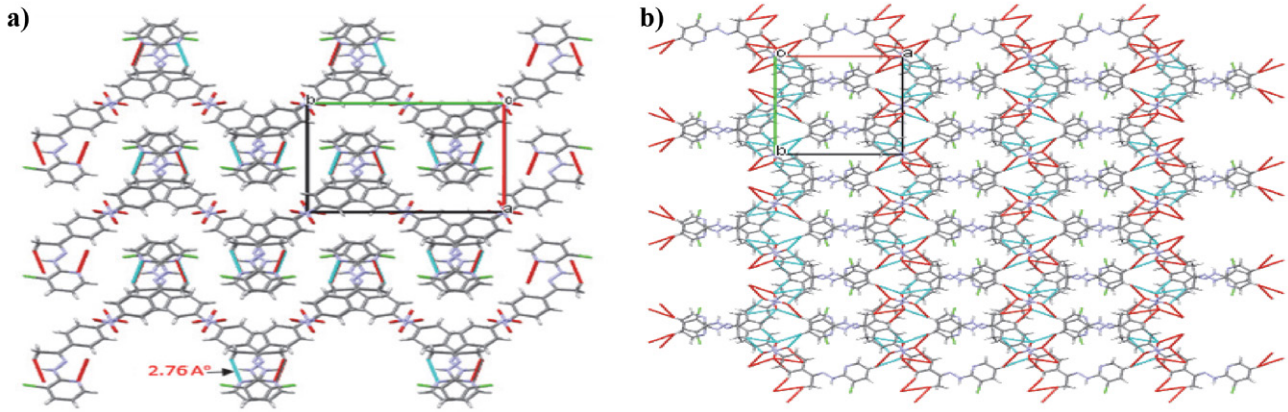

Fig. 3. a) Two-dimensional self-assembling; b) three-dimensional supramolecular frameworks of $C_{13}H_{11}ClN_4O_2$ and hydrogen bonds

3. 2. ^{1}H NMR Studies

^{1}H-NMR spectrum of HL_1 is shown in Fig. 4. ^{1}H-NMR spectrum of the HL_1 ligand oxime (N–OH) group of the proton (H13) was observed at 9.83 ppm as a singlet peak. The NH proton (H8) generated a signal at 8.45 ppm. The spectrum of the (2*E*,3*Z*)-3-[2-(3-chloropyridin-2-yl)hydrazinylidene]-*N*-hydroxybutan-2-imine ligand observed at singlet peaks 2.23 ppm (H14A, H14B, H14C) and 2.34 ppm (H15A, H15B, H15C) methylene group of protons. While H1 proton signal appeared at d 8.37 ppm, the signals at d 7.62 and d 6.84 ppm were due to H3 and H2 of pyridinium moiety, respectively.[32] In HL_2, the NH proton (H7) generated a sharp signal at 8.48 ppm, as a singlet peak. The peaks were observed at range 8.30–6.84 ppm were assignable to the protons of aromatic rings as multiplet peaks. The spectrum of the 3-chloro-2-{(2*Z*)-2-[1-(4-nitrophenyl)ethylidene]hydrazinyl}pyridine ligand observed at singlet peaks 2.38 ppm (H10A, H10B, H10C) methylene group of protons. The signal at d 8.30 ppm was attributed at to (H6) aromatic proton of pyridine. The proton signal appearing at d 8.20 and d 8.01 ppm were due to (H13, H17, H16, H14) of aromatic moiety respectively. Aromatic protons of pyridine moiety produced a broad signal at d 7.61 and t 6.84 ppm (H5, H4).[11,18,33] It was observed that the obtained results were exactly compatible with the structure.

3. 3. ^{13}C NMR Studies

^{13}C-NMR spectrum of HL_1 is shown in Fig. 5. ^{13}C-NMR spectrum HL_1 observed a single resonance at 157.39 and 157.32 ppm, respectively which showed that the oxime (C=NOH) and hydrazone (-NHN=CH) (C11,C10) carbon atoms. All the signals were assigned to the aromatic carbons (C1-C5) of the pyridine at the range of 150.00–115.35 ppm. The signals observed at 10.03 and 9.53 ppm are attributable to the carbon atom of methyl group (C15,C14). For HL_2, aromatic carbons of pyridine and benzene rings gave different signals in their resonance. Hence the signals at 149.92, 147.61, 137.33, 116.97, 115.49 ppm were due to carbon (C2-C6) while (C12-C17) presented in different signals at 144.49, 144.42, 126.89, 126.89, 123.64, 123.64 ppm in the aromatic moiety of ligand. Two equivalent para carbons (C13,C17) and (C14,C16) brought out a signals at d 126.89 and 123.64 ppm in the spectrum. The signal at 147.17 ppm was due to the (C9) carbon of the imine group of moiety. The signal observed at 12.53 ppm is attributable to the carbon atom of methyl group (C10).[25,32,33]

3. 4. UV-Vis Absorption Spectra and TD-DFT Calculations

UV-Vis calculations were performed by TD-DFT/B3LYP method with 6-31G basis set using Gaussian 09

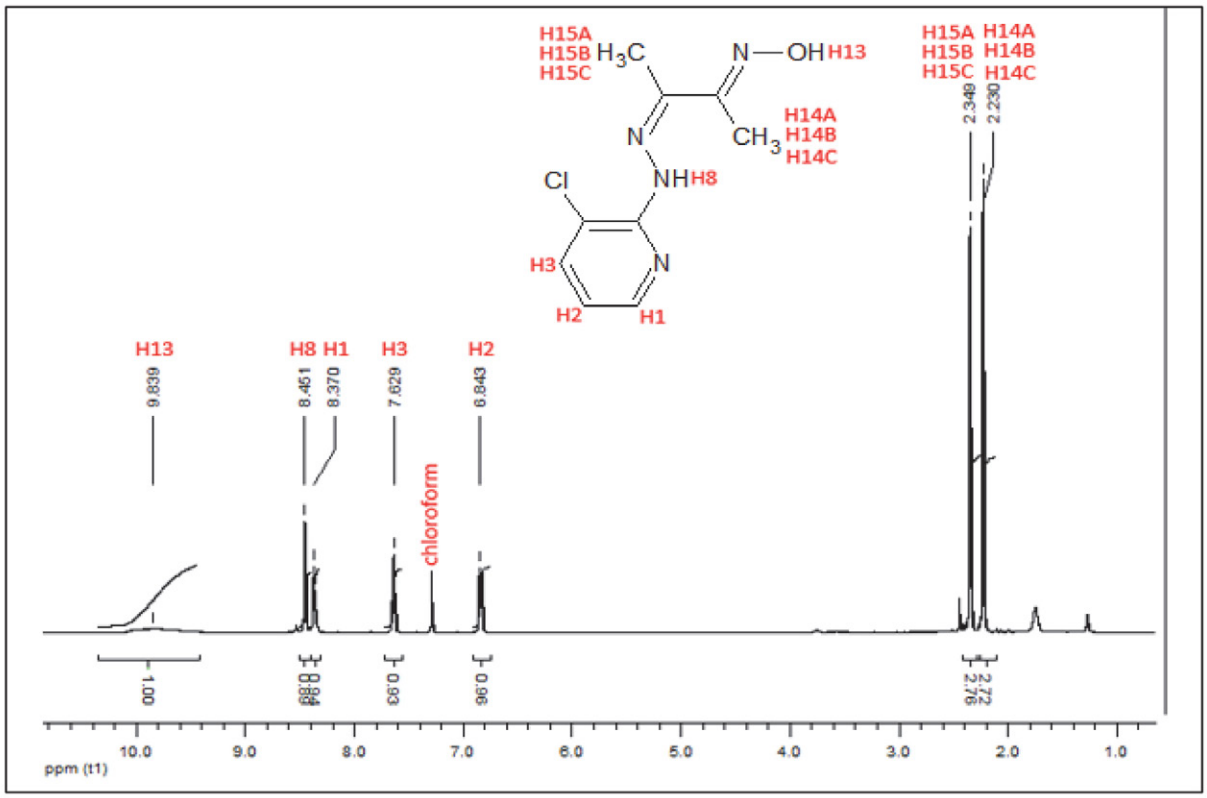

Fig. 4. ^{1}H-NMR spectrum of HL_1

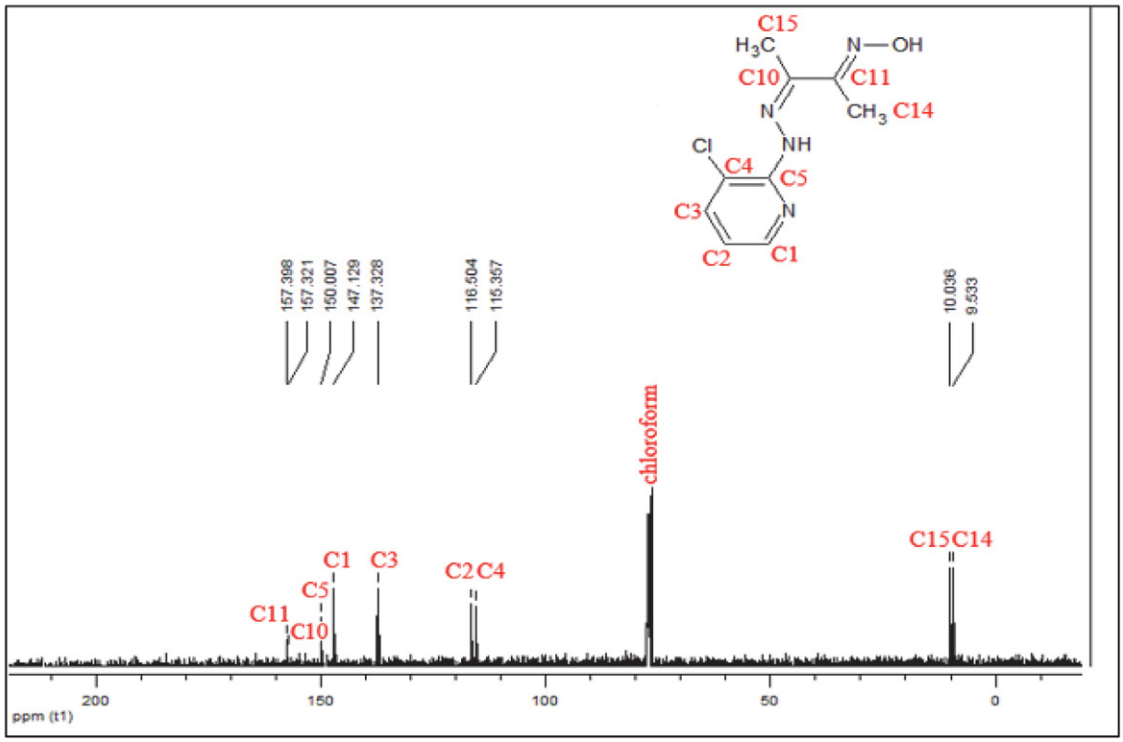

Fig. 5. ^{13}C-NMR spectrum of HL_1

program.[34,35] The electronic absorption spectra of the ligands, along with the molar extinction coefficient, were obtained in a 5 × 10^{-5} mol L^{-1} chloroform solution in the wavelength zone (240–480 nm) using the spectroscopic method.[23] The electron transition possibilities of different compounds were compared using ultraviolet-visible spectroscopy. For HL_1 and HL_2, slightly different absorption peaks centered at 322, 285 nm and 362, 312 nm (ε = 42800, 41100 and 34520, 26300 mol^{-1} L cm^{-1}), respectively. The experimental UV-Vis spectra of the HL_1 compund and corresponding theoretical calculations are plotted in Fig. 6. Theoretical calculations predicted two peaks at 307, 287 nm and 364, 331 nm which indicated formation of the HL_1 and HL_2.[36] The calculated excitation energy, excitation wavelength, oscillator strength with the aid of TD-DFT/B3LYP method are given in Table 4. The electronic absorption spectra of the ligands were defined with two sharp absorption bands. These two bands were observed at 285-312 and 322–362 nm indicative of the π-π* and n-π* transitions, respectively.[37] While the π-π* transitions of the ligands originated from the electrons of the pyridine ring, the n-π* band occurred due to hydrazone groups (-NHN=CH) of atoms.[38]

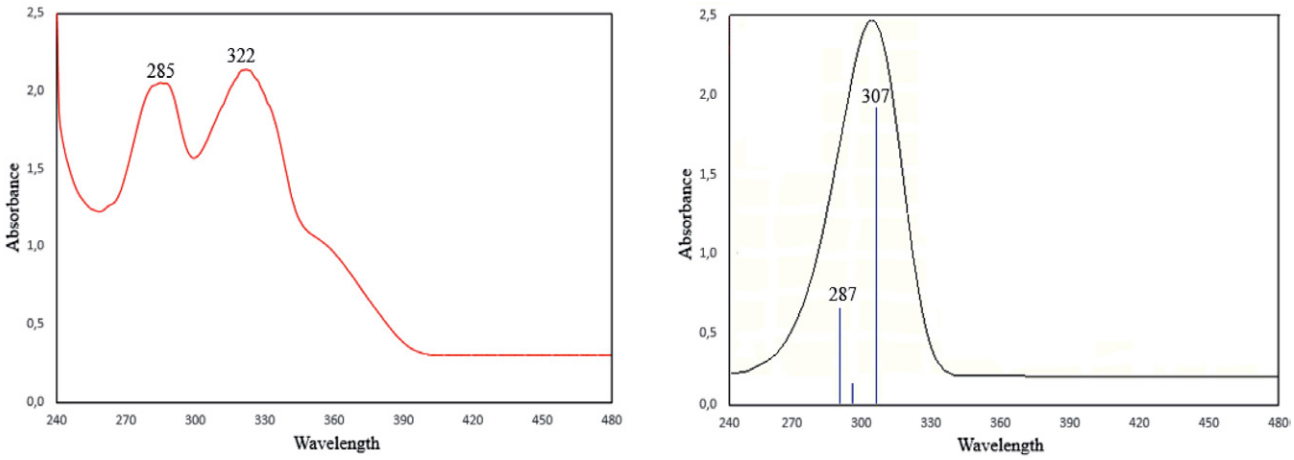

Fig. 6. The (left) experimental and (right) calculated spectrum and observed UltravioleteVisible spectra of the HL_1 in CH_2Cl_2 solution at room temperature

Table 4. The experimental and calculated UV-Vis spectral parameters for HL_1 and HL_2 ligand with its assignments.

Compounds	Experimental λ(nm)	Calculated λ(nm)	E (eV)	f	Assignment
HL_1	285	287	4.36	0.18	π-π*
	322	307	4.03	0.03	n-π*
HL_2	312	331	3.73	0.02	π-π*
	362	364	2.56	0.06	n-π*

3. 5. Mass and FT-IR Spectra

Mass spectral datas of ligands were obtained by electrospray ionization (ESI) method. The mass exhibited the molecular ion at m/z 226.66284 $[M+1]^+$ and 290.70558 $[M+1]^+$ which indicated formation of the HL_1 and HL_2 (Fig. S1). The moleculer peak of both ligands have a 100% relative abundance.[32]

Generally compunds are characterized by three IR absorption bands such as ν(O–H), ν(C=N) and ν(N–O) stretching vibrations. FT-IR spectrum of the HL_1 ligand showed (C=N) imine (C=N) oxime peaks at 1596 cm^{-1} and 1516 cm^{-1} (Fig. S2).[39] The bands 3361 cm^{-1} and 3377 cm^{-1} were due to (N-H) vibrations for HL_1 and HL_2 respectively. Also (O-H) band of oxime group peak was observed at 3111 cm^{-1}.[33] But this peak was not seen at HL_2 ligand. At the same time, the bands at 935 cm^{-1} and 1392 cm^{-1} assignable to (N-O) and (NO_2) vibrations, respectively. The FT-IR spectrum of ligands displayed bands at 2981 cm^{-1} and 2972 cm^{-1} which assignable to ($C\text{-}H_{Ar}$) protons. The medium bands observed at 553 cm^{-1} and 546 cm^{-1} assigned to pyridyl rings. For HL_1 and HL_2, the bands 1454–1451 cm^{-1}, 1394–1392 cm^{-1}, 1044–1032 cm^{-1} and 1012–1032 cm^{-1} assignable to the aromatic pyridine ring.[40] FT-IR analysis give us the preliminary information about whether this structure is formed or not. Our datas are in agreement with similar oxime and pyridine ligands in the literature.[41]

3. 6. Hirshfeld Surface Analysis

The surface analysis method is the best way to identify crystal packing and intermolecular interacting in a structure. For this reason, the Hirshfeld surface analysis was performed using CrystalExplorer software (version 17.5).[42,43] Accordingly, the close correlations between the fragments were quantitatively analyzed. Furthermore, it is one of the computer calculation programs to investigate the mechanism of molecular interactions in proteins and with which intermolecular interactions they could bond to a receptor. In addition, it helps to identify the intermolecular hydrogen bond as well as π-π, C-H···X (X=halogens) interactions with great importance in crystal package arrangement and stabilization of the molecule. Therefore, C(17)-H(17)···O(20) and C(13)-H(13)···Cl(11) interactions are illustrated in Fig. 7.

Intermolecular interactions of HL_2 ligand is presented in Fig. 8 as 2D fingerprints plot.[44] Blue zone shows intermolecular interaction areas whereas grey zone shows outside of the this interaction area. According to fingerplots studies results of for HL_2; Cl···H 11,4%, H···H 28,7%, N···C 6,4%, N···H 6,5%, O···H 18,3%, Cl···N 2,5%, C···C 3,8%, C···H 15,2%.[22–24] Other bondings constituted all interactions by making small contributions on the surface. The highest H···H interaction rate (28.7%) was shown to be derived from the abundance of the H···H interactions in aromatic rings (Fig. S3).[4]

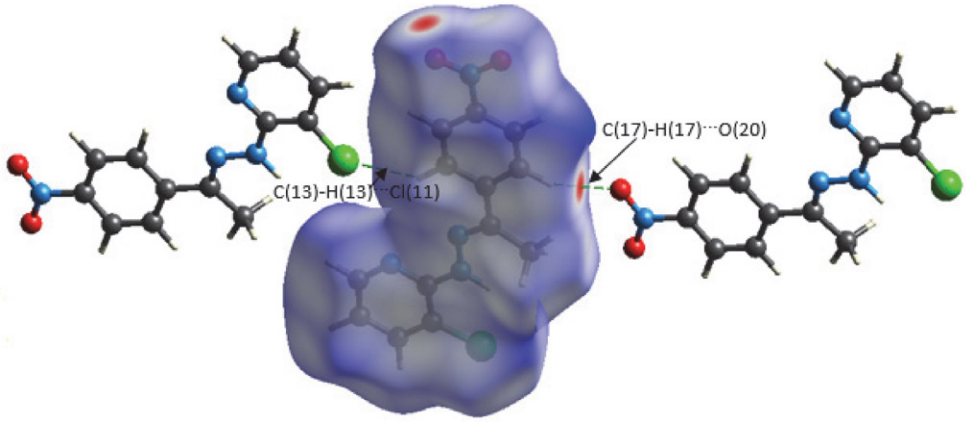

Fig. 7. Close contact of C(17)-H(17)···O(20) and C(13)-H(13)···Cl(11) interactions determined by Hirshfeld surface analysis over dnorm of HL_2

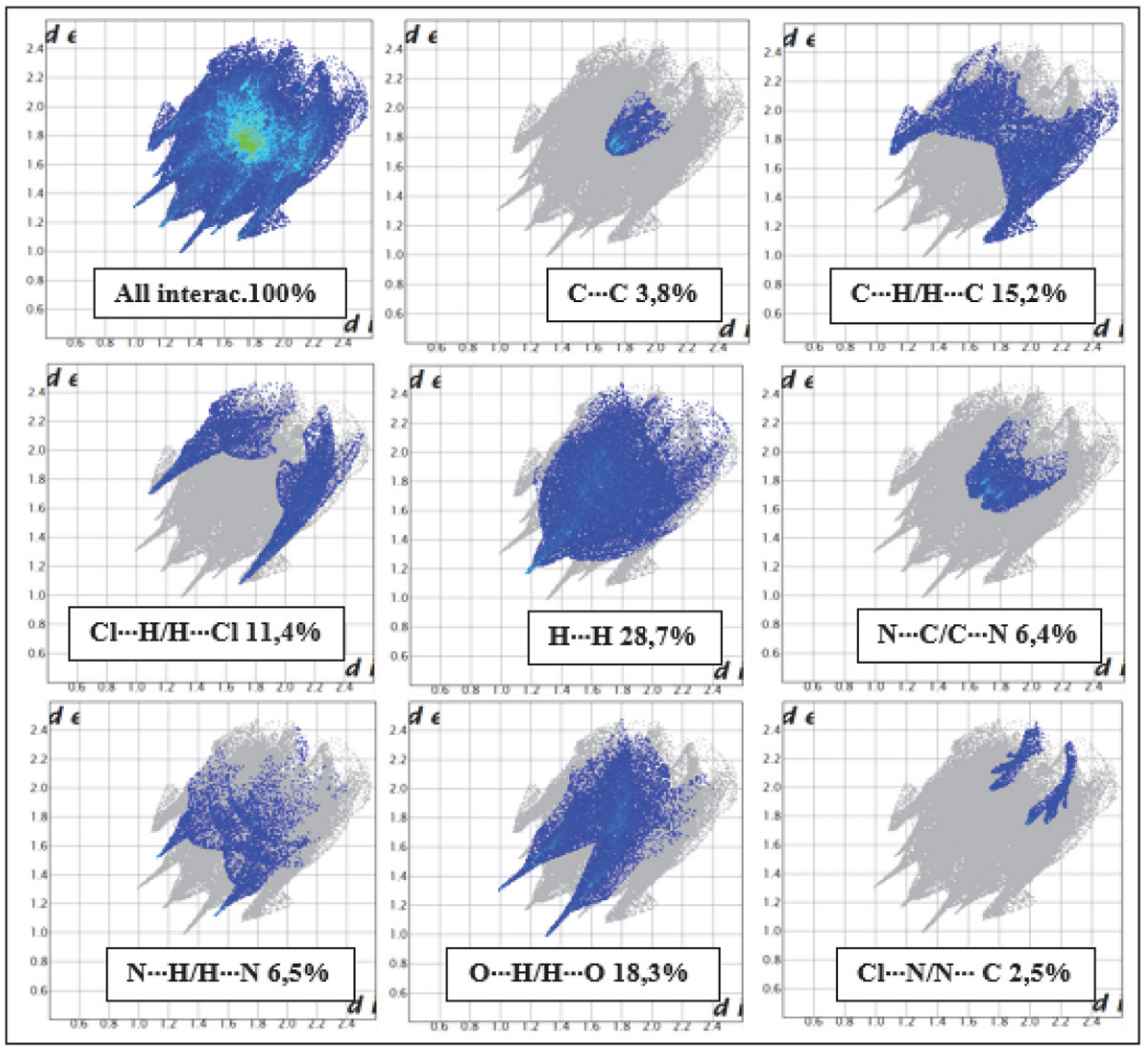

Fig. 8. The 2D fingerprint plos of the HL_2

3. 7. Molecular Electrostatic Potential Analysis

Molecular electrostatic potential mapping is a method for the observation of the interactions of molecules with each other based on their charge distribution on 3D diagrams. This is an auxiliary method that estimates electrophilic and nucleophilic reactive sites of ligands leading to investigate protein binding and medicine developing by defining hydrogen bond interactions.[4,45] Electrostatic po-

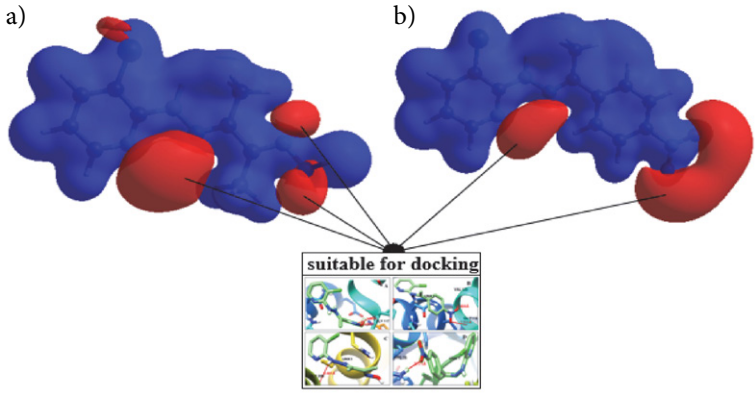

Fig. 9. Electrostatic potential maps of a) $C_9H_{11}ClN_4O$ and b) $C_{13}H_{11}ClN_4O_2$

tential (3D) diagrams of ligands were mapped using the Hartree-Fock theory Slater type orbital-3G base set of Hirshfeld surface analysis by CrystalExplorer software as depicted in Fig. 9. The input file of the geometry was obtained using Tonto.[46,47] Surface qualification values were set –0,025–0,025 au and high resolution was selected. When it was performed, the molecule was taken to transparency mode and atoms were made clear. The red color represents the negative electrostatic potential regions and acceptor hydrogen bonds. Moreover, the blue color represents the positive electrostatic potential regions and donor hydrogen bonds.[48,49] In addition, blue-colored zones are the preferred regions for the nucleophilic attack, while red-colored negative zones are susceptible to electrophilic attack.[11] Furthermore, red-colored regions have electron-rich atoms or atom groups; therefore, they can easily interact with amino acid residues. Based on the findings of molecular docking studies, hydrogen bond interactions between donor-acceptor confirmed the results of the electrostatic potential analysis as depicted in Fig. 11.

3. 8. Molecular Docking Studies

In silico docking calculations are of great importance in drug design and medical chemistry fields. Molecular docking is commonly used in the studies carried out on target medicine designing by estimating the binding mechanisms of small molecules on target biologic proteins.[50,51] Donor-acceptor binding mechanisms create complexations with hydrophobic hydrogen bond and electrostatic interactions.[52] The current study examined the ligands creating intramolecular hydrogen bonds by targeting the active zones of *E. coli* DNA GyrB (PDB Code:4WUB) and *E. coli* FabH (PDB Code:1HNJ) amino acid residues. The protein-related data were obtained from Research Collaboratory for Structural Bioinformatics Protein Data Bank https://www.pdb.org. Molecular docking studies analyzed binding energy, hydrogen bonding, and interactions between the ligands and bacteria.[53–56] Furthermore, by the calculation of the ligands' lowest binding energy to aminoacids residues, it was determined that which structure has stronger hydrogen bonding and higher binding energy score.[57] Ligands SMILES formats were created at page https://www.cheminfo.org; it is C/C(=N\O)/C(C)=N/Nc1ncccc1Cl for HL_1 and C/C(=N/Nc1nccc1Cl)c2ccc(N(=O)=O)cc2 for HL_2.

Molecular docking studies were performed Autodock vina program (https://www.vina.scripps.edu). Ligands were converted into mol2 format and prepared for molecular docking at Chimera software program with receptors (*E.coli* FabH and GyrB) (https://www.cgl.ucsf.edu/chimera/).[58] In the Dock Prep method, firstly, all nonstandarts and solvents were selected and refined from receptors. Then, protein models were added by the selection of all hydrogen atoms (also considered H-bonds) and Gasteiger charges. Docking studies were conducted by targeting ligand receptors and binding the most convenient coordinates.[59] While defining an approximate donor and acceptor binding zone in in-silico studies, docking parameters are of great importance. Different types of grid box values were applied for the best and most accurate binding. The application of target protein binding zones (as a great scale) in a cubic box resulted in the best binding; however, this method requires a long computer calculation.[60,61] The grid box values of ligands applied to *E. coli* GyrB receptor were 10, 25, –10 at the center with a grad spacing of 0.375 Å including default the sizes of 40, 40, 40 for HL_1 and HL_2. The same method was employed to *E. coli* FabH receptor reporting the values of 30, 15, 30 at the center with the sizes of 30, 30, 30 for HL_1 and HL_2. In addition, default values were used for other parameters. Root-mean-square deviation were selected as minumum value. The binding energy values of –7.9 and –8.8 kcal/mol were applied by HL_1 and HL_2 ligands to the GyrB receptor, respectively. Fig. 10 illustrates the hydrophobicity surface area of HL_1 inside GyrB and FabH proteins. The binding energy values

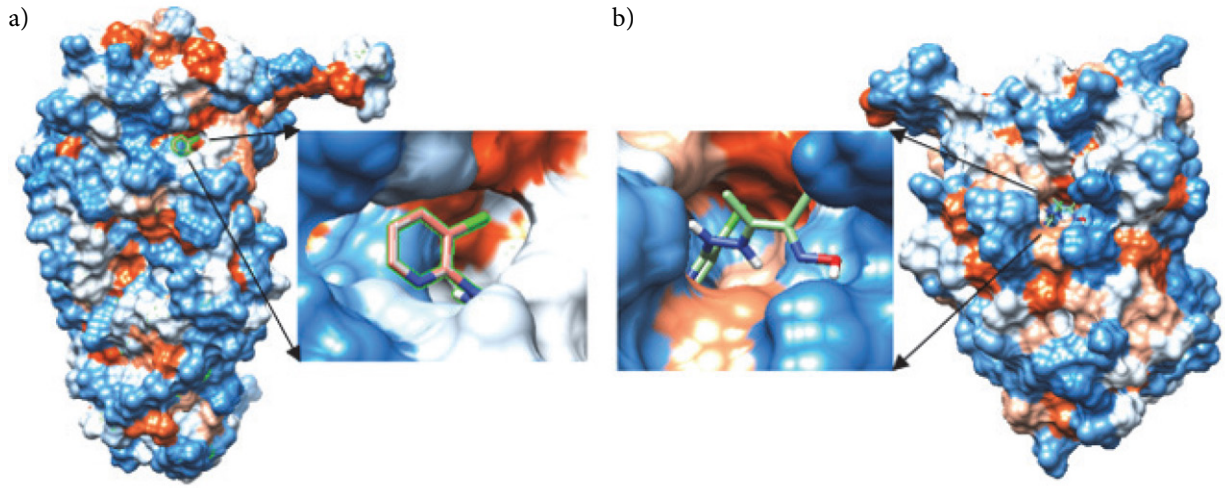

Fig. 10. Illustration of hydrophobicity surface area of HL_1 inside a) gyrase subunit B and b) beta-ketoacyl-acyl carrier protein synthase III proteins

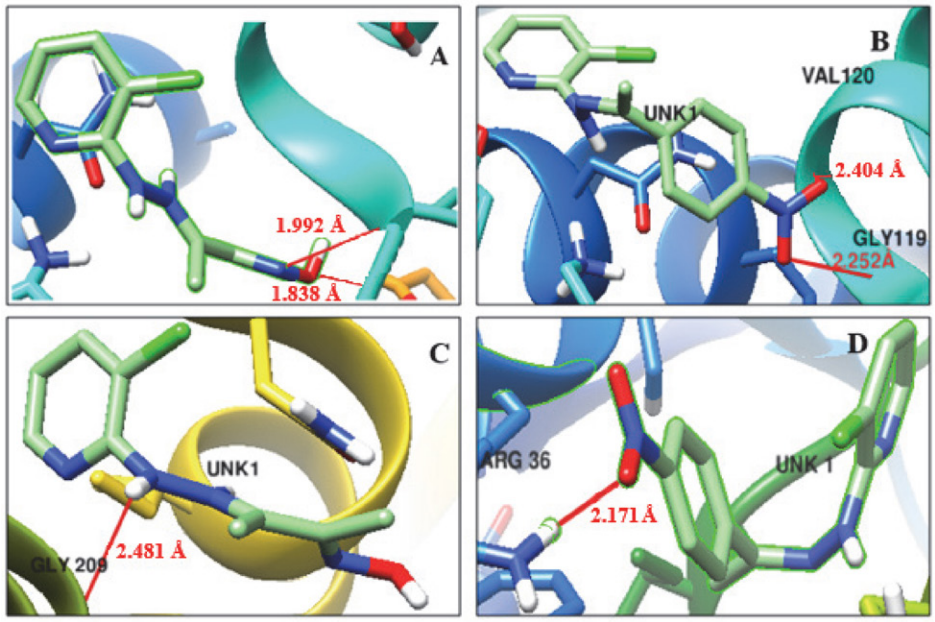

Fig. 11. Results of molecular docking for a) HL_1-gyrase subunit B (GyrB) (4WUB), b) HL_2-GyrB (4WUB), c) HL_1- beta-ketoacyl-acyl carrier protein synthase III (FabH) (1HNJ), and d) HL_2-FabH (1HNJ)

of –6.1 and –6.8 kcal/mol were applied by HL_1 and HL_2 ligands to the FabH receptor, respectively. The binding interactions and docking poses are depicted in Fig. 11. Since the ligands bind to the GyrB receptor with higher binding energy than that reported for the FabH receptor, there was a better docking to the ligands-GyrB complex. While there were two hydrogen bonds in the complex that ligands made with 4WUB protein, 1HNJ protein had one hydrogen bond. This finding proved that this effect increases the binding energy value. As the binding energy value enhances, the binding score increases indicating a better docking.[41,62] Therefore, the binding energy of HL_2 was higher than that reported for HL_1 which is considered a better docking. The other reason behind that is believed to be the electron density and unpaired electron couples of two oxygen atoms that bond to the nitrogen atom of HL_2.[63] In a study carried out by Fathima et al. (2018), docking results were observed to be –8.4 and –8.5 kcal/mol for 2ABP2C-1HNJ and 2ABHB-1HNJ, respectively.[54]

The HL_1 created a hydrogen bond to GLY 117 and GLN 335.A HE22 amino acid residues of 4WUB protein with N12 and O13 atoms and binding lengths were observed as 1.992 Å and 1.838 Å, respectively. The HL_2 bonded to GLY 119 and VAL 120 amino acid residues of 4WUB proteins with O19 and O20 atoms and binding lengths were observed as 2.252 Å and 2.404 Å. In another study conducted by Metelytsia et al. (2020), the binding of ligands to the regions of amino acid residues were reported as GLY 119 and His 116. This finding is similar to the results of docking investigations in the current study in terms of attachment regions.[52] The HL_1 and HL_2 created a hydrogen bond to GLY 209, ARG 36.A HH22 amino acid residues of 1HNJ receptor with N8 and O19 atoms and binding lengths were observed as 2.481 Å and 2.171 Å, respectively. Donor and acceptor hydrogen binding interactions are shown as Table 5.[64] The findings of docking studies confirmed that the results and interactions of molecular electrostatic potential generally occur in red regions. The

Table 5. AutoDock results showing Compound-Protein name, Binding site of protein, Binding site of Ligand, Type of interactions, Bond length, Binding energy.

Compound-Protein name	Binding site of protein	Binding site of Ligand	Type of interaction	Bond length (Å)	Binding energy (Kcal/Mol)
HL_1-4WUB	GLY 117	UNK1-N12 atom	Hydrogen bond	1.992	–7.9
	GLN 335.A HE22	UNK1-O13 atom	Hydrogen bond	1.838	
HL_2-4WUB	GLY 119	UNK1-O19 atom	Hydrogen bond	2.252	–8.8
	VAL 120	UNK1-O20 atom	Hydrogen bond	2.404	
HL_1- 1HNJ	GLY 209	UNK1-N8 atom	Hydrogen bond	2.481	–6.1
HL_2- 1HNJ	ARG 36.A HH22	UNK1-O19 atom	Hydrogen bond	2.171	–6.8

findings of docking studies also revealed that ligands are potential inhibitors against *E. coli* DNA GyrB and *E. coli* FabH.[65]

3. 9 Drug-Likeness and Biological Activity

Drug-likeness and bioactivity of ligands were obtained from molinspiration (https://www.molinspiration.com/cgi-bin/properties). Although the parameters of druglikeness cannot estimate the biological activity of each compound, it is one of the most successful and efficient methods for the analysis of compounds with medicinal potential through the determination of pharmacokinetic characteristics. Based on Table 6, the parameters of drug-likeness and biologic activity for the compounds in the present study (miLogP, TPSA, nAtoms, MW, nON, nOHNH, nviolations, and rotb) and (enzyme inhibitor, protease inhibitor, nuclear receptor ligand, kinase inhibitor, ion channel modulator, and GPRC ligand). The aforementioned findings have been the first obtained data regarding the medicinal potential of the compounds.[66] The values of drug-likeness were determined in this study, and the ligands were examined regarding midicinal potential with the consideration of these values. In this sense, the miLogP parameter, which is the capacity of penetrating the cell membrane, is expected to be under 5. In this regard, the values of miLogP parameter were reported as 1.81 and 3.37 for HL_1 and HL_2, respectively. The polar surface area (TPSA) represents the hydrogen bonding potential of a compound. Accordingly, the TPSA values were observed as 69.88 and 83.11 A^2 for HL_1 and HL_2, respectively. These values were below the 160 A^2 limit defined for TPSA and at a good performance.[67–70] Although miLogP and TPSA are not sufficient criteria for the investigation of druglikeness, they are two important parameters to represent oral absorption in cells.[71] The number of acceptor hydrogen bonds was set to nON ≤ 10, and the number of donor hydrogen bonds was set to nOHNH ≤ 5. In this study, the obtained results were below the aforementioned values.[72] Low molecule weight is important in terms of easy transport, diffusion, and absorption of the molecule. The values of molecular weight are expected to be < 500 Da. In this study, the molecular weights of the ligands were lower than the aforementioned value. The ligands were reported with successful results according to Lipinski's rule of five. Based on Fig. 12, the red column shows Lipinski's rule of five, and the green and red columns depict the druglikeness score of the ligands.[68]

If the value of violations equals 0, it shows that crystallized compounds can easily bond to the receptor. This value was reported as 0 for the compounds of the present study. The number of rotatable bonds is a simple topological value and measurement of flexibility.[73] If the bioactivity results of the compounds are > 0, –5.0-0.0, and < –5.0, they are considered active, medium active, and not active, respectively. All the results of biological activity parameters were within the range of –5.0–0.0; therefore, the ligandswere regarded as medium active.[74] As a result, it was concluded that the ligands of the current study obtained satisfactory druglikeness scores and properties to be considered medicine potential agents.

Table 6. Calculated drug-likeness parametres and Bioactivity Score of ligands.

	HL_1	HL_2
$miLog_P$	1.81	3.37
TPSA	69.88	83.11
natoms	15	20
MW	226,67	290.71
nON	5	6
nOHNH	2	1
nviolations	0	0
nrotb	3	4
GPCR ligand	–0.78	–0.70
Ion channel modulator	–0.62	–0.70
Kinase inhibitor	–0.74	–0.55
Nuclear receptor ligand	–1.32	–0.94
Protease inhibitor	–1.32	–1.02
Enzyme inhibitor	–0.43	–0.49

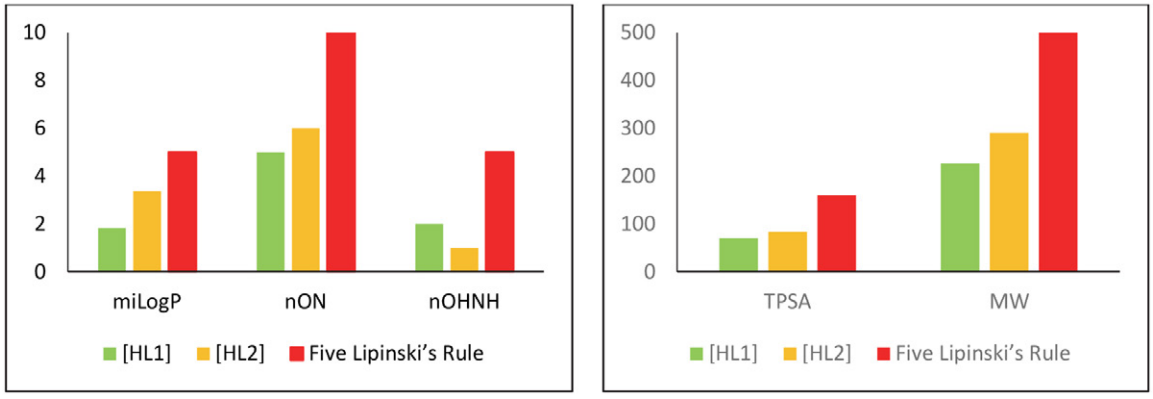

Fig. 12. Druglikeness scores of ligands according to Lipinski's rule of five

4. Conclusion

In this work, the new (2*E*,3*Z*)-3-[2-(3-chloropyridin-2-yl)hydrazinylidene]-*N*-hydroxybutan-2-imine and 3-chloro-2-{(2*Z*)-2-[1-(4-nitrophenyl)ethylidene]hydrazinyl}pyridine ligands were synthesized and characterized by elemental analysis, LC/MS-MS, FT-IR, ^{1}H-NMR, ^{13}C-NMR and UV-Vis. HL_2 was also determinated by single-crystal X-ray diffraction (XRD) and crystallized in the space group $P2_1/c$ of with Z=4 and was linked into (3-D) network by C-H···O intermoleculer hydrogen bonding interactions. Additionally, Cl···H 11,4%, H···H 28,7%, N···C 6,4%, N···H 6,5%, O···H 18,3%, Cl···N 2,5%, C···C 3,8%, C···H 15,2% reciprocal influence were revealed by Hirshfeld Surface Analysis. The mass spectra of the ligands showed the main peaks that corresponding to $[M+1]^+$. UV-Vis studies demonsrated that the π-π* and n-π* transitions appearing at 285, 312 nm and 322, 362 nm, respectively. The obtained experimental results of the present study were fully compatible with the theoretical results. The binding energy values of –7.9 and –8.8 kcal/mol were applied by HL_1 and HL_2 ligands to the GyrB receptor, respectively. Moreover, the binding energy values of –6.1 and –6.8 kcal/mol were applied by HL_1 and HL_2 ligands to the FabH receptor. The increase at binding energy values is resulted with a better docking. Therefore, HL_2 has a better docking ability than HL_1. The synthesized ligands are compatible with Lipinski's rule of five and have features to be a good drug-likeness scores. The bioactivity scores of the ligands are within the range of –5.0-0.0; consequently, the pharmacokinetic and pharmacological properties of the ligands are appropriate leading to be considered potential drug agents.

5. References

1. H. Mansouri-Torshizi, M. Moghadam, A. Divsalar and A. Saboury, *Acta Chim. Slov.*, **2011**, *58*, 811–822.
2. E. Gina Vasile Scăet, M. C. Chifiriuc, C. Bleotu, C. Kamerzan, T. Luminița Măru, C. G. Daniliuc, C. Maxim, L. Calu, R. Olar and M. Badea, *Molecules*, **2018**, *23*, 1–18. **DOI:**10.3390/molecules23010157
3. B. A. V Lima, A. E. Graminha, A. Kuznetsov, J. Ellena, F. R. Pavan, C. Q. F. Leite and A. A. Batista, *J. Braz. Chem. Soc.*, **2016**, *27*, 30–40. **DOI:**10.5935/0103-5053.20150237
4. M. Venkateshan, R. V. Priya, M. Muthu, J. Suresh and R. R. Kumar, *Chem. Data Collect.*, **2019**, *23*, 100262. **DOI:**10.1016/j.cdc.2019.100262
5. L. Metelytsia, D. Hodyna, I. Dobrodub, I. Semenyuta, M. Zavhorodnii, V. Blagodatny, V. Kovalishyn and O. Brazhko, *Comput. Biol. Chem.*, **2020**, *85*, 107224. **DOI:**10.1016/j.compbiolchem.2020.107224
6. S. S. Kumar, S. Athimoolam and B. Sridhar, *Spectrochim. Acta. A. Mol. Biomol. Spectrosc.*, **2015**, *146*, 204–213. **DOI:**10.1016/j.saa.2015.02.104
7. A. M. Netto, S. M. C. M. Bicalho, C. L. Filgueiras and J. C. Machado, *Chem. Phys. Lett.*, **1985**, *119*, 507–510. **DOI:**10.1016/0009-2614(85)85378-1
8. N. Wazzan, *Asian J. Chem.*, **2015**, *27*, 4641–4656. **DOI:**10.14233/ajchem.2015.19304
9. G. Vadivelan, M. Saravanabhavan, V. Murugesan and M. Sekar, *Spectrochim. Acta. A. Mol. Biomol. Spectrosc.*, **2015**, *145*, 461–466. **DOI:**10.1016/j.saa.2015.03.045
10. K. M, S. Saxena, R. S and V. R, *Curr. Med. Chem. - Anti-Infective Agents*, **2003**, *2*, 269–286. **DOI:**10.2174/1568012033483015
11. S. Madhankumar, P. Muthuraja and M. Dhandapani, *J. Mol. Struct.*, **2020**, *1201*, 127151. **DOI:**10.1016/j.molstruc.2019.127151
12. M. Akram, S. Niaz, M. Adeel, M. N. Tahir, I. Ullah, M. A. Ullah, S. Subashchandrabose and G. Uddin, *J. Mol. Struct.*, **2019**, 127448. **DOI:**10.1016/j.molstruc.2019.127448
13. L. K. McLellan and D. A. Hunstad, *Trends Mol. Med.*, **2016**, *22*, 946–957. **DOI:**10.1016/j.molmed.2016.09.003
14. V. L. Tchesnokova, L. L. Ottley, K. Sakamoto, J. Fierer, E. Sokurenko and M. A. Liss, *Urology*, **2015**, *86*, 1200–1205. **DOI:**10.1016/j.urology.2015.07.008
15. Y. Zhang, X. Zhang, L. Qiao, Z. Ding, X. Hang, B. Qin, J. Song and J. Huang, *J. Mol. Struct.*, **2019**, *1176*, 335–345. **DOI:**10.1016/j.molstruc.2018.08.069
16. K. M. Hillgren, A. Kato and R. T. Borchardt, *Med. Res. Rev.*, **1995**, *15*, 83–109. **DOI:**10.1002/med.2610150202
17. N. Srinivasan, S. Thirumaran and S. Ciattini, *J. Mol. Struct.*, **2009**, *936*, 234–238. **DOI:**10.1016/j.molstruc.2009.08.001
18. B. Guhathakurta, C. Biswas, J. P. Naskar, L. Lu and M. Zhu, *J. Chem. Crystallogr.*, **2011**, *41*, 1355–1359. **DOI:**10.1007/s10870-011-0103-x
19. O. V Dolomanov, L. J. Bourhis, R. J. Gildea, J. A. K. Howard and H. Puschmann, *J. Appl. Crystallogr.,* **2009**, *42*, 339–341. **DOI:**10.1107/S0021889808042726
20. L. Palatinus, S. J. Prathapa and S. van Smaalen, *J. Appl. Crystallogr.*, **2012**, *45*, 575–580. **DOI:**10.1107/S0021889812016068
21. C. F. Macrae, I. J. Bruno, J. A. Chisholm, P. R. Edgington, P. McCabe, E. Pidcock, L. Rodriguez-Monge, R. Taylor, J. Van De Streek and P. A. Wood, *J. Appl. Crystallogr.*, **2008**, *41*, 466–470. **DOI:**10.1107/S0021889807067908
22. E. Matamala-Cea, F. Valenzuela-Godoy, D. González, R. Arancibia, V. Dorcet, J. R. Hamon and N. Novoa, *J. Mol. Struct.*, **2020,** *1201*, 127139. **DOI:**10.1016/j.molstruc.2019.127139
23. Y. Y. Cai, L. Y. Xu, L. Q. Chai and Y. X. Li, *J. Mol. Struct.*, **2020**, *1204*, 127552. **DOI:**10.1016/j.molstruc.2019.127552
24. Q. Wu, Y. Tang and Q. Zi, *Polyhedron*, **2019**, *166*, 123–129. **DOI:**10.1016/j.poly.2019.03.021
25. N. Bandyopadhyay, A. B. Pradhan, S. Das, L. Lu, M. Zhu, S. Chowdhury and J. P. Naskar, *J. Photochem. Photobiol. B Biol.*, **2016**, *160*, 336–346. **DOI:**10.1016/j.jphotobiol.2016.04.026
26. S. Chantrapromma, P. Jansrisewangwong and H.-K. Fun, *Acta Crystallogr. Sect. E. Struct. Rep. Online*, **2010**, *66*, o2994-5. **DOI:**10.1107/S1600536810043266

27. T. Karakurt, S. Meral, A. A. Agar, *Süleyman Demirel Univ. J. Nat. Appl. Sci.,* **2019**, *23*, 505–514. **DOI:**10.19113/sdufenbed.530279
28. E. Szłyk, A. Wojtczak, A. Surdykowski and M. Goździkiewicz, *Inorganica Chim. Acta*, **2005**, *358*, 467–475. **DOI:**10.1016/j.ica.2004.07.065
29. L. Chai, Y. Zhang, J. Tong and G. Liu, *Z. Naturforsch.,* **2013**, *68b*, 239–244. **DOI:**10.5560/znb.2013-2301
30. P. Pattanayak, J. L. Pratihar, D. Patra, P. Brandão and V. Felix, *Inorganica Chim. Acta*, **2014**, *418*, 171–179. **DOI:**10.1016/j.ica.2014.04.021
31. H. Wang, H. Xiao, N. Liu, B. Zhang and Q. Shi, *Open J. Inorg. Chem.*, **2015**, *05*, 63–73. **DOI:**10.4236/ojic.2015.53008
32. T. Topal, E. Karapınar, *J. Turkish Chem. Soc. Sect. A Chem.*, **2018**, *5*, 785–802. **DOI:**10.18596/jotcsa.324878
33. T. Topal, H. H. Kart, P. Tunay Taşlı and E. Karapınar, *Opt. Spectrosc.,* **2015**, *118*, 897–912. **DOI:**10.1134/S0030400X15060223
34. M. J. Frisch *et al.,* G16_B01. *Gaussian 16, Revision B.01* Gaussian, Inc., Wallingford CT, **2016**.
35. J. B. Foresman, A. E. Frisch., Exploring chemistry with electronic structure methods. *Gaussian, Inc.,* **1996**.
36. R. Mohamed Asath, R. Premkumar, T. Mathavan and A. Milton Franklin Benial, *Spectrochim. Acta - Part A Mol. Biomol. Spectrosc.*, **2017**, *175*, 51–60. **DOI:**10.1016/j.molstruc.2017.04.117
37. E. Erdem, M. Akarsu, R. Kılınçarslan, İ. Kayağil, İ. Kara and S. Söyleyici, *Croat. Chem. Acta,* **2016**, *89*, 55–64. **DOI:**10.5562/cca2820
38. S. Shit, M. Nandy, C. Rizzoli and S. Mitra, *J. Chem. Sci.,* **2016**, *128*, 913–920. **DOI:**10.1007/s12039-016-1082-4
39. E. Karapinar, O. Karabulut and N. Karapinar, *Hindawi Publ. Corp. J. Chem.* **2013**, 2013. **DOI:**10.1155/2013/256983
40. H. Briseño-Ortega, L. Juárez-Guerra, S. Rojas-Lima, L. H. Mendoza-Huizar, R. A. Vázquez-García, N. Farfán, R. Arcos-Ramos, R. Santillan and H. López-Ruiz, *J. Mol. Struct.,* **2018**, *1157*, 119–126. **DOI:**10.1016/j.molstruc.2017.12.059
41. R. Mohamed Asath, R. Premkumar, T. Mathavan and A. Milton Franklin Benial, *Spectrochim. Acta - Part A Mol. Biomol. Spectrosc.*, **2017**, *175*, 51–60. **DOI:**10.1016/j.saa.2016.11.037
42. P. Muthuraja, M. Sethuram, T. Shanmugavadivu and M. Dhandapani, *J. Mol. Struct.*, **2016**, *1122*, 146–156. **DOI:**10.1016/j.molstruc.2016.05.083
43. M. A. Spackman and D. Jayatilaka, *CrystEngComm*, **2009**, *11*, 19–32. **DOI:**10.1039/B818330A
44. J. J. McKinnon, M. A. Spackman and A. S. Mitchell, *Acta Crystallogr. Sect. B.*, **2004**, *60*, 627–668. **DOI:**10.1107/S0108768104020300
45. R. Daengngern and N. Kungwan, *J. Lumin.*, **2015**, *167*, 132–139. **DOI:**10.1016/j.jlumin.2015.06.001
46. J. J. McKinnon, D. Jayatilaka and M. A. Spackman, *Chem. Commun.*, **2007**, 3814–3816. **DOI:**10.1039/b704980c
47. D. Jayatilaka and D. J. Grimwood, *Comput. Sci. ICCS,* **2003**, 142–151. **DOI:**10.1007/3-540-44864-0_15
48. M. A. Spackman, J. J. McKinnon and D. Jayatilaka, *CrystEngComm*, **2008**, *10*, 377–388. **DOI:**10.1039/b715227b
49. S. M. Kumar, B. C. Manjunath, G. S. Lingaraju, M. M. M. Abdoh and M. P. Sadashiva, *Cryst. Struct. Theory Appl.* **2013**, *2013*, 124–131. **DOI:**10.4236/csta.2013.23017
50. S. Vilar, G. Cozza and S. Moro, *Curr. Top. Med. Chem.*, **2008**, *8*, 1555–1572. **DOI:**10.2174/156802608786786624
51. R. Thomsen and M. H. Christensen, *J. Med. Chem.*, **2006**, *49*, 3315–3321. **DOI:**10.1021/jm051197e
52. P. Sjoberg and P. Politzer, *J. Phys. Chem.*, **1990**, *94*, 3959–3961. **DOI:**10.1021/j100373a017
53. E. G. Sağlam, E. Bulat, C. T. Zeyrek, H. Dal and T. Hökelek, *J. Mol. Struct.*, **2019**, *1178*, 112–125. **DOI:**10.1016/j.molstruc.2018.09.084
54. K. S. F. M. Sathiyendran, K. Anitha, *Mater. Sci. Eng. C.*, **2018**, *91*, 103–114. **DOI:**10.1016/j.msec.2018.05.035
55. I. Ali, M. N. Lone, Z. A. Alothman and A. Alwarthan, *J. Mol. Liq.*, **2017**, *234*, 391–402. **DOI:**10.1016/j.molliq.2017.03.112
56. M. M. Silva, F. C. Savariz, E. F. Silva-JÃ\textordmasculinenior, T. M. de Aquino, M. H. Sarragiotto, J. C. C. Santos and I. M. Figueiredo, *J. Braz. Chem. Soc.*, **2016**, *27*, 1558–1568.
57. M. K. Bhattacharyya, D. Dutta, S. M. Nashre-ul-Islam, A. Frontera, P. Sharma, A. K. Verma and A. Das, *Inorganica Chim. Acta*, **2020**, *501*, 119233. **DOI:**10.1016/j.ica.2019.119233
58. R. S. Soderquist and A. Eastman, *Mol. Cancer Ther.*, **2016**, *15*, 2011–2017. **DOI:**10.1158/1535-7163.MCT-16-0031
59. N. Shahabadi and M. Falsafi, *Spectrochim. Acta - Part A Mol. Biomol. Spectrosc.*, **2014**, *125*, 154–159. **DOI:**10.1016/j.saa.2014.01.066
60. W. P. Feinstein and M. Brylinski, *J. Cheminform.*, **2015**, *7*. **DOI:**10.1186/s13321-015-0067-5
61. D. Plewczynski, M. Lazniewski, R. Augustyniak and K. Ginalski, *J. Comput. Chem.*, **2011**, *32*, 742–755. **DOI:**10.1002/jcc.21643
62. B. Kurt, H. Temel, M. Atlan and S. Kaya, *J. Mol. Struct.,* **2020**, *1209*, 127928. **DOI:**10.1016/j.molstruc.2020.127928
63. N. Das, P. K. Jena and S. K. Pradhan, *Heliyon*, 2020, **6**, e02693. **DOI:**10.1016/j.heliyon.2019.e02693
64. A. De, H. P. Ray, P. Jain, H. Kaur and N. Singh, *J. Mol. Struct.*, **2020**, *1199*, 126901. **DOI:**10.1016/j.molstruc.2019.126901
65. M. Parveen, A. Aslam, A. Ahmad, M. Alam, M. R. Silva and P. S. P. Silva, *J. Mol. Struct.*, **2020**, *1200*, 127067. **DOI:**10.1016/j.molstruc.2019.127067
66. S. M. Hiremath, A. S. Patil, C. S. Hiremath, M. Basangouda, S. S. Khemalapure, N. R. Patil, S. B. Radder, S. J. Armaković and S. Armaković, *J. Mol. Struct.*, **2019**, *1178*, 1–17. **DOI:**10.1016/j.molstruc.2018.10.007
67. C. A. Lipinski, F. Lombardo, B. W. Dominy and P. J. Feeney, *Adv. Drug Deliv. Rev.* **2001**, *46*, 3–26. **DOI:**10.1016/S0169-409X(00)00129-0
68. C. A. Lipinski, *Drug Discov. Today. Technol.*, **2004**, *1*, 337–341. **DOI:**10.1016/j.ddtec.2004.11.007
69. A. Verma, *Asian Pac. J. Trop. Biomed.*, **2012**, *2*, 1735–1737. **DOI:**10.1016/S2221-1691(12)60486-9
70. P. Ertl, B. Rohde and P. Selzer, *J. Med. Chem.*, **2000**, *43*, 3714–3717. **DOI:**10.1021/jm000942e

71. S. Nadeem, M. Sirajuddin, S. Ahmad, S. A. Tirmizi, M. I. Ali and A. Hameed, *Alexandria J. Med.*, **2016**, *52*, 279–288. **DOI:**10.1016/j.ajme.2015.10.003
72. S. Deswal, Naveen, R. K. Tittal, D. Ghule Vikas, K. Lal and A. Kumar, *J. Mol. Struct.*, **2020**, *1209*, 127982. **DOI:**10.1016/j.molstruc.2020.127982
73. D. F. Veber, S. R. Johnson, H.-Y. Cheng, B. R. Smith, K. W. Ward and K. D. Kopple, *J. Med. Chem.*, **2002**, *45*, 2615–2623. **DOI:**10.1021/jm020017n
74. N. Dege, A. S. Aydın, E. Ağar, S. Kansız, S. JoseKavitha, K. BalaSubramani, M. Hemamalini and V. Rajakannan, *Chem. Data Collect.*, **2020**, *25*, 100320. **DOI:**10.1016/j.cdc.2019.100320

Povzetek

A detailed description of the two new pyridine ligands, (2E**,**3Z**)**-3-[2-(3-chloropyridin-2-yl)hydrazinylidene]-N-hydroxybutan-2-imine and 3-chloro-2-{(2Z)-2-[1-(4 nitrophenyl)ethylidene]hydrazinyl}, is reported. The synthesized compounds were characterized by spectroscopic studies, spectral features were performed by TD-DFT calculations. New-generation pyridine ligand of HL_2 was also determinate by single-crystal X-ray diffraction and Hirshfeld surface analysis with two-dimensional fingerprint plots was used to analyze intermolecular interactions in crystals. Molecular-docking was performed to investigate the binding areas of chemical compounds, and the results showed the inhibitory activity of the studied HL_1 and HL_2 against *E. coli***.** The results of the current study revealed the drug-likeness and bioactive properties of the ligands.

Podan je podroben opis dveh novih piridinskih ligandov, (2E,3Z)-3-[2-(3-kloropiridin-2-il) hidraziniliden]-N-hidroksibutan-2-imina in 3-kloro-2-{(2Z)-2-[1-(4nitrofenil)etiliden] hidrazinila}. Sintetizirane spojine so bile okarakterizirane s spektroskopskimi študijami, spektralne značilnosti pa so bile ovrednotene z izračuni TD-DFT. Nova generacija piridinskih ligandov HL2 je bila določena tudi z žarkovno rentgensko difrakcijo, za analizo medmolekularnih interakcij v kristalih pa je bila uporabljena Hirshfeldova površinska analiza s specifičnimi dvodimenzionalnimi prikazi. Za proučitev vezavnih površin kemijskih spojin smo izvedli molekularno sidranje, pri čemer so rezultati pokazali inhibitorno aktivnost proučevanih HL_1 in HL_2 spojin napram *E. coli*. Rezultati sedanje študije kažejo na potencialne zdravilne in bioaktivne lastnosti ligandov.